Published in final edited form as:

Electrophoresis. 2017 October ; 38(19): 2374–2388. doi:10.1002/elps.201700114.

Fabrication Techniques Enabling Ultrathin Nanostructured Membranes for Separations

Marcela Mireles Ramirez and **Thomas R. Gaborski**

Rochester Institute of Technology, Biomedical Engineering Department

Abstract

The fabrication of nanostructured materials is an area of continuous improvement and innovative techniques that fulfill the demand of many fields of research and development. The continuously decreasing size of the smallest patternable feature has expanded the catalog of methods enabling the fabrication of nanostructured materials. Several of these nanofabrication techniques have sprouted from applications requiring nanoporous membranes such as molecular separations, cell culture, and plasmonics. This review summarizes methods that successfully produce through-pores in ultrathin films exhibiting an approximate pore size to thickness ratio of one, which has been shown to be beneficial due to high permeability and improved separation potential. The material reviewed includes large-area, parallel, and affordable approaches such as self-organizing polymers, nanosphere lithography, anodization, nanoimprint lithography as well as others such as solid phase crystallization and nanosphere lens lithography. The aim of this review is to provide a set of inexpensive fabrication techniques to produce nanostructured materials exhibiting pores ranging from 10 to 350 nm and exhibiting a pore size to thickness ratio close to one. The fabrication methods described in this work have reported the successful manufacture of nanoporous membranes exhibiting the ideal characteristics to improve selectivity and permeability when applied as separation media in ultrafiltration.

Keywords

nanofabrication; nanoporous; membrane; nanostructured; ultrafiltration

1. Introduction

Separations of biological and chemical species has great value in industrial processes, biopharmaceutical production, medical care, and water purification. Semipermeable membranes that are classified as ultrafiltration sieves, with approximately 10–100 nm pores, are commonly used to address these needs [1]. Conventional polymeric ultrafiltration membranes are limited in their ability to separate two or more species similar in size due in part to a log-normal distribution of pore sizes [2]. Tortuous path polymeric membranes also have significant surface area that can lead to adsorption and loss of desired product [3]. Additionally, most ultrafiltration membranes are orders of magnitude thicker than the pore diameter resulting in low permeability [4]. Improvements in nanofabrication and recent

Corresponding author: Thomas R. Gaborski, 160 Lomb Memorial Drive, Rochester NY 14623, trgbme@rit.edu, Fax: 585-475-5041.

interest in nanomanufacturing offer promise in making significant improvements in ultrafiltration [5]. The ideal molecular or protein sieve is a membrane with a uniform distribution of pores in an ultrathin film, while fabricated and supported in a manner that is scalable and robust enough for practice use. Through-pores and the use of inorganic materials might also enable membranes that can be cleaned, sterilized, and reused far more readily than tortuous path polymeric membranes currently in use today.

The classic Mehta and Zydney Selectivity-Permeability plot has long predicted an upper bound on selectivity for ultrafiltration membranes with log-normal distributions of pores [6]. While uniform pore size or isopore membranes currently exist that would push the limits of this plot, such as commercially available track-etched membranes, their low porosity and significant thickness results in very low permeability [7,8]. Ultrathin membranes, ≤ 100 nm thickness, present unique transport efficiency not normally found in much thicker polymeric membranes considered in the Mehta and Zydney plot. At membrane thicknesses below roughly 100 nm, the diffusive flux of molecular species through the pores can be comparable to the convective flux, leading to a Peclet number of approximately one [8]. Not only is the convective flux through the ultrathin membranes much greater than conventional filters due to higher hydraulic permeability, but diffusion presents an important enhancement that is no longer insignificant and can even exceed convective transport [9]. Diffusion based separations are also critically important in laboratory and medical applications among others. The transport of blood toxins across dialysis membranes is predominantly diffusive because of limited transmembrane pressure and the desire to remove a calculated water volume. Ultrathin membranes have been theoretically and experimentally shown to impart minimal resistance to diffusion while also enabling higher resolution separations prior to reaching equilibrium [4,10]. The potential performance enhancements in selectivity and permeability of ultrathin membranes will lead to not only faster and better separations, but potentially revolutionize current separation approaches and enable new devices such as wearable hemodialyzers [11,12].

Precise size exclusion and permeability are two important characteristics that a membrane must exhibit in order to be successfully applied in chemical and biological processes [13,14]. The ideal nanofabrication method should allow controlling feature size and distribution while providing a large area of fabrication to ensure mass manufacture feasibility [5]. Fabrication techniques can be divided into two categories according to their overall approach being top-down or bottom-up; Figure 1 shows a schematic comparison of these two directions. Top-down processes allow closer control on feature size and distribution; however, their high cost often limits their application. In contrast, bottom-up processes are more affordable and although feature size and distribution is, to some degree limited, these processes provide a good trade-off between cost and functionality.

Traditionally, micro and nanofabrication methods follow a top-down approach as in photolithography, allowing the reshaping of a macroscopic layer into an array of microscopic features with excellent control in shape, size, and distribution. Electron and ion beam lithography are examples of top-down approaches regarded as serial processes. These methods overcome the intrinsic resolution limit dictated by the wavelength of the light used in conventional photolithography, offering outstanding control at the nanometer scale [15].

Nanoporous membranes have been successfully fabricated through this approach on silicon nitride with pores as small as 25 nm in diameter [12]. Nevertheless, the throughput of this top-down serial approach remains low, resulting in significant cost.

The electronics industry continues to drive the innovation sustaining the advancement of top-down fabrication technologies through parallel processes, achieving a feature size well below 14 nm when developing the latest technology node using energetic lasers [16]. Similar technologies are based on the use of X-rays, laser interference, ultraviolet and extreme ultraviolet light which are impractical for the low-cost production of large-area nanostructured materials that would be neccesary for chemical and biological separations [17,18]. Another top-down parallel approach is the ionic track etching technique based on the irradiation of a sample. A porous pattern is revealed after etching the nuclear tracks with ultimate pore diameters ranging from 10 nm to 10 μm. This technique is used to produce the commercially available polymeric track-etched membranes commonly applied in filtration processes and for cell culture [19]. Similarly, the process has been used on thin silicon nitride films to produce a free-standing membrane with pore sizes <20 nm [20]. Nevertheless, this technique requires access to a particle accelerator capable of generating energies up to GeV which often results in an unstable particle flux [19]. Moreover, the random nature of this technique limits its precision and pattern versatility leading to a trade-off between low porosity and merged doublet pores [21]. Finally, nanoimprint lithography is recognized as the most affordable top-down parralel aproach, often limited only by the high cost of the master mold required to imprint a nanoscale pattern. The cost of this top-down technique has been reduced through the optimum design of the thermal budget during processing [22].

In summary, conventionally used high cost top-down nanofabrication methods, serial and parallel, remain an unlikely candidate for the advancement of low-cost and large-area membrane fabrication. Conversely, bottom-up approaches allow the formation of arrays of nanoscopic features through the use of atomic, molecular or particle building blocks, often resulting in a parallel process. These are efficient and spontaneous processes that under the right conditions promote materials self-structuring into nanoscale patterns that can be controlled through indirect environmental parameters.

This review will discuss processes that have enabled the fabrication of nanostructured membranes at a reasonable cost, highlighting those producing released or free-standing membranes with a pore size to thickness aspect ratio close to one. These techniques have been utilized to produce membranes with thicknesses in the range of 70–540 nm, demonstrating the feasibility and great potential of achieving ultrathin membrane fabrication. Table 1 summarizes pore dimensions and aspect ratio of the highlighted membrane reports. The use of self-organizing polymers [23–29] and nanosphere lithography [30–35] are discussed first; these methods are being increasingly applied for ultrathin membrane fabrication. Nanosphere lithography can be considered a hybrid approach; however, it is based on a bottom-up self-assembly of nanospheres. Anodization [36–40] will be presented next; although, not widely applied for the fabrication of ultrathin membranes, this very well researched process has been successfully used for the production of nanoporous patterns and thick membranes. Although commonly considered a top-down

approach, nanoimprint [41–43] techniques that utilize low-cost or unique master molds have been included in this review. Finally, an overview of other applied or developing fabrication methods is also offered. Figure 2 shows micrographs adapted from publications reporting the production of membranes processed through the nanofabrication techniques reviewed in this work. These techniques correspond to bottom-up or affordable top-down strategies which are favorable for the production of nanoscale patterns over large-areas at low-cost. The aim of this review is to provide a critical analysis of nanofabrication methods enabling the production of ultrathin nanoporous membranes to be used as separation media.

2. Challenges of bottom-up membrane fabrication

Bottom-up techniques provide a platform for the production of porous patterns at the nanoscale. One of the major quality and usability challenges when applying these patterns for the fabrication of separation membranes is the presence of defects. Point defects found in porous membranes can be summarized as defects resulting in pore absence as well as defects resulting in altered pore size. The absence of pores can potentially increase flow resistance while reducing yield; however, this will not significantly hinder the functionality of the membrane. On the other hand, the variation in pore size or merging of pores directly impacts the selectivity by allowing unwanted particles to move across the membrane, which can compromise its functionality, particularly in applications such as virus removal in bioprocessing. Simple methods can be implemented to tune the pore size distribution. Decreasing the pore size can be accomplished by placing a conformal layer through techniques such as atomic layer deposition. Increasing the pore size is often achieved by isotropic etching in wet or dry chemistries. Change in thickness should be considered when applying these tuning methods.

In self-organizing polymers, the defect concentration has been related to the Flory-Huggins interaction parameter (χ) which is related to microphase separation, a system with a large χ will be more likely to undergo microphase separation and develop fewer defects [95]. Templated self-assembly has been used to promote long-range order in self-organizing polymers by using templated substrates that guide the arrangement and decrease the defect concentration. The templates consist of shallow steps; however, sidewall defects in the template can lead to domain vacancies and changes in the width can create dislocations; both point defects contribute to the absence of pores [96], an acceptable defect for separations.

Nanosphere lithography is based on the periodic arrangement of nanoparticles over a monolayer which can represent a challenge. Polydisperse solutions of nanoparticles translate into polydisperse pore sizes. Overabundant quantities of nanoparticles, hinder the formation of monolayers which can potentially result in larger pore sizes. Both effects result in defects related to pore size and significantly affect separation processes based on size. Several methods addressing the periodicity of the assembled beads have been reported [67,97]. Another factor increasing the concentration of defects is the plasma treatment used to decrease particle size. This type of defect arises from the formation of a pedestal that results in the nanoparticles tipping over to a side [35], which has a minimal effect on pore arrangement and does not generally impact membrane functionality.

In the case of anodization, the most common defect is disorder of the generated pores which is affected by the anodizing voltage, temperature, solution, and pre-existing defects in the metallic substrate used [98], [99]. High-purity aluminum foils yield nanoporous structures with a higher ordering degree than low-purity aluminum or aluminum alloys. Long term anodization can increase the order by rearranging the pores [40]. However, the improved order might be the result of pore enlargement [100], a type of defect that directly affects the size exclusion capability of a membrane.

Defects occurring in nanoimprint lithography can be repeated or random [101]. Repeated defects are those created from a defective nanoimprint master mold; random defects are those produced as a result of particles, non-uniform contact or residue. The non-uniformity causes incomplete pattern development due to non-ideal contact with the mold. Presence of residue arises from the adhesion of the polymer to the mold. The latter can be minimized with the use of a fluorinated monolayer to decrease the surface energy of the mold [102]; however, the anti-adhesive character has been found to decrease when in contact with air [103]. Non-uniformity and residue cause the increase of defects related to pore size which have a detrimental effect on membranes applied as separation media.

Defects have many origins and achieving a defect-free membrane is impractical. Therefore it is important to study the defect concentration related to a particular nanofabrication route. These versatile techniques can be integrated into processes enabling the fabrication of organic and inorganic based membranes; where the active area closely depends not only on the fabrication method but on properties such as strength and stability of the selected membrane material. As usual, optimization must be application driven since it is the application which determines the active area, type and level of accepted defects.

3. Self-organizing polymers

Traditional ultrafiltration membranes typically made by solvent casting polymeric materials have been used and studied for several decades. These asymmetric membranes have a selective skin over a mechanically strong porous substructure [26]. Parameters such as a solvent to polymer ratio, temperature, and gelation medium effectively control the characteristics of the resulting membranes [46]. However, these membranes exhibit a tortuous pore structure which increases flow resistance and surface area, impacting the flow and resulting in product loss. The self-organizing quality of polymers has attracted much interest since it provides an efficient path for the formation of nanostructures exhibiting well aligned and through-pores. The most studied self-organizing polymers are the block copolymers (BCP), macromolecules composed of two or more distinct units that undergo microphase separation due to their positive enthalpy of mixing; hence self-organizing into well-defined arrays in the nanoscale [47,48]. Membrane fabrication technologies have benefited from BCP research, applying its findings into the fabrication of nanopores. After the polymers undergo self-organization, removing one of the components in the array results in nanostructured porous materials [49].

Self-organizing BCP is a versatile technology yielding nanoporous membranes of polymeric nature such as polystyrene (PS) or poly (methyl methacrylate) (PMMA); and non-polymeric

nature such as silicon nitride (Si_3N_4). The general fabrication process can be divided into three main steps. First the BCPs are synthesized in solution, then the solution is deposited on a substrate to self-organize creating discrete domains and finally, one domain is removed. A simple method such as spin coating stands as the most widely used BCP deposition technique; however, drop-casting or immersion of the substrate in the BCP solution has also been reported [53]. Additionally, the process offers the option of transferring the pattern to an underlying material.

After self-organization, the polymers yield a film with discrete domains perpendicularly oriented to the substrate [14,47]; or above a critical concentration, aggregation results in micelles of an insoluble core with a soluble outer ring [52]. Therefore, pairing the BCP with the ideal solvent and optimizing the concentration plays an important role in achieving a determined BCP nanoarchitecture.

Polystyrene-block-poly(ethylene oxide) (PEO) was used by Altinpinar *et al.* [47] to produce PS membranes supported on silicon wafers. The use of UV light as a cleaving agent was reported. Ortho-nitrobenzyl ester was used as the BCP junction which was later photocleaved. The PEO was washed in ultrapure water to reveal the nanoporous PS layer exhibiting 10 nm pores with a thickness of 24 nm. It is important to mention that the washing process distorted the morphology of the nanoporous film obtained; therefore, further investigation is required. Moreover, the nanoporous films remained supported on the silicon wafer; hence, integration of a releasing step is also required.

A PMMA membrane was successfully lifted-off a silicon wafer and transferred onto a microfiltration membrane (Figure 3a). In this case, the addition of PMMA homopolymer caused the BCP to self-organize around the PMMA homopolymer cylindrical structures which was then removed in acetic acid. The latter resulted in a nanoporous PS-PMMA film supported on a sacrificial silicon oxide (SiO_2) layer dissolved in hydrofluoric acid (HF). The released membrane was transferred to a microfiltration polysulfone membrane. The obtained nanoporous membrane exhibited 15 nm pores with a thickness of 80 nm. The process was reported and applied by Yang *et al.* [14] to produce a device designed for the retention of human rhinovirus type 14 (HRV14) 30 nm in size. The virus was successfully separated from a solution containing bovine serum albumin (BSA) 7 nm in size. Regardless of the very thick (150 μm) microfiltration membrane used as a support, the authors reported high flux when compared against a polycarbonate track-etched membrane.

The fabrication of another double-layered filtration device was reported by Nuxoll *et al.* [51], where a polymeric nanoporous membrane was fabricated on a Si_3N_4/Si microporous support (Figure 3b). The method involved a PS-poly(isoprene)-poly(lactide) (PS-PI-PLA) triblock copolymer spin coated onto a Si_3N_4 surface, where the polymeric mixture self-organized into PI-PLA cylinders perpendicular to the substrate and embedded in a PS continuous layer. Then, the PLA domain was removed to reveal a nanoporous pattern exhibiting 45 nm pores with a thickness of 80 nm. Micrographs taken with a scanning electron microscope (SEM) showed irregularly shaped pores due to fluoropolymer deposition during reactive ion etch (RIE). Nevertheless, the authors demonstrated a successful nanofabrication method to produce a double-layered filtration device that showed

a 50-fold increased selectivity of methyl orange over dextran blue when compared against an anodized alumina membrane (60 μm thick and 200 nm pores). The increased selectivity was attributed to improved hydrodynamic interaction with the nanopore walls.

Montagne *et al.* [5], reported the fabrication of a Si_3N_4 membrane through the use of self-assembled micelles (Figure 3c). The micellar arrangement represents a negative template and therefore must be inverted before it can be directly transferred to create nanopores. After etching the polymeric residue between micelles, the pattern was transferred into an underlying silicon film. The latter results in silicon nanopillars on top of a Si_3N_4 film. A chromium thin film was then selectively deposited on the Si_3N_4 only and the silicon nanopillars dissolved in potassium hydroxide (KOH), leaving a chromium layer with a nanoporous pattern which was then transferred into the Si_3N_4 through RIE. Finally, the back of the wafer was etched by deep-RIE (DRIE) to yield a free standing membrane with 95 nm pores and a thickness of 100 nm; showing improved transport rate compared to track-etched membranes.

Popa *et al.* [52], followed a similar micellar approach by using polystyrene-block-poly(2-vinylpyridine) (PS-P2VP) deposited on a full $4''$ silicon wafer previously coated with SiO_2 followed by 100 nm of Si_3N_4 (Figure 3d). A thin chromium etching template was produced in a similar fashion as described above and transferred into the Si_3N_4 layer to produce 80 nm pores with a thickness of 100 nm. The membrane release was accomplished by a KOH through-wafer etch that created exposed membrane windows. The SiO_2 film was used as an etch stop to prevent etching of the membrane; lastly, the SiO_2 was removed by a quick buffered oxide etch (BOE). In sum, the authors reported a nanofabrication process executed at the wafer scale (50% yield) containing several 10x10 μm^2 nanoporous membranes.

BCPs are able to attain several different nanopatterns, hence it is important to exert control over their self-organizing process. Several scientific reviews have tackled the task of outlining the chemical and physical details governing BPC technology [23,24,27–29]. Solvent evaporation or annealing,[54] applied electric field,[55] chemical (chemoepitaxy) or topographical (graphoepitaxy) treatment of surfaces are a few examples of strategies developed for the control of the self-organization of BCPs [23,24]. The dimensions of the domains or micelles formed in the self-organized BCPs films determines the size and distribution of the pores; which can be tuned by varying the molecular weight as well as the deposition parameters such as spinning speed, humidity, and temperature [5,52].

Overall, several research groups have demonstrated a straightforward BPC process for the fabrication of ultrathin free-standing or released nanoporous membranes that are integrated with conventional silicon technologies. The scalable nature of semiconductor manufacturing gives promise for the production of ultrathin membranes using these approaches.

4. Nanosphere lithography

Nanosphere lithography (NSL) is a patterning process that has been used and developed for the past three decades. It is a simple and inexpensive method that has found many applications in the fabrication of nanostructured materials [35]. This technique enables

spheres to be used as templates to create nanoscale features. Most employed spheres are polystyrene but the use of silica has also been reported. In addition to producing nanoporous membranes, this technique has been used to produce silicon nanopillar arrays for fuel cells [56], chromium nanorings potentially applicable to optical and electro-optical devices [57], plasmonic patterns on graphene [58], gold nanohole arrays for electrochemical sensors [59], among many others.

A solution containing the spheres is first prepared to then be deposited on a surface where the self-assembly forms a 2D colloidal crystal film with hexagonal symmetry [35]. Spin-coating, drop casting, dip coating, electrochemical or electrophoretic deposition, assembly at an interface and template-guided assembly are some deposition techniques used [32,63]. Many works have aimed to expand the control over the order of the nanospheres by depositing them on substrates placed at a tilt angle [32]. Additionally, controlled size reduction of the nanospheres after deposition has also been reported through the use of isotropic plasma etching; achieving a 65% reduction in diameter [64]. This shrinking effect is a simple and reliable process employed to achieve smaller feature sizes and increased spacing between features. Non-optimal etching parameters result in heterogeneous size and shape as well as the movement of the nanospheres and ultimately loss of symmetry [63].

After deposition and post-treatment of the nanospheres, the areas that are left uncovered are most commonly etched for pattern transfer; however, Kang *et al.* [60] functionalized them in order to selectively direct the deposition of a modified poly(hydroxyethyl methacrylate) (PHEMA) hydrogel to those open areas between nanospheres (Figure 4a). A porous hydrogel was obtained exhibiting ~215 nm pores with a thickness of ~75 nm as estimated from atomic force microscopy micrographs. The produced nanoporous hydrogel membrane was detached from the substrate by UV-initiated cleavage. After membrane detachment, the authors reported a thickness decrease of about 2.5 to 3 times and an increase in pore diameter due to lateral stretching.

A more commonly taken approach is to etch the open areas which transfers the nanospheres pattern into an underlying film. This results in nanodots (2D) or nanopillars (3D) depending on the etch depth; hence, the pattern must be inverted in order to produce nanopores. The latter can be accomplished by deposition of a metallic film on top of the nanospheres; followed by their removal usually assisted by sonication. The process results in a nanoporous metallic layer which can then be used as an etch mask for pattern transfer. This was the approach taken by Klein *et al.* [61] in order to produce Si_3N_4 nanoporous membranes (Figure 4b). The authors employed PS spheres that underwent a RIE process in an oxygen atmosphere to reduce their size. A thin chromium layer was used to produce the nanoporous etch mask to transfer the pattern into an underlying Si_3N_4 film. After membrane release in a KOH bath to etch the exposed silicon wafer from the backside, free-standing membranes exhibiting 350 nm pores with a thickness of 100 nm as estimated from SEM micrographs were obtained.

Interestingly, NSL has also been used to aid in the anodization of aluminum. Lipson *et al.* [62] reported a fabrication process for creating a nanoporous tungsten pattern on an aluminum layer deposited on silicon, acting as an etch mask to create ordered aluminum pits

(Figure 4c). After tungsten removal, anodization was performed as a one-step process to produce 70 nm pores with a thickness of 300 nm. This work demonstrates an efficient approach to ensure vertical sidewalls on anodized aluminum oxide (AAO), an alternative to the usual two-step anodization commonly used to achieve the same goal.

Finally, Acikgoz *et al.* [44], employed silica nanoparticles assembled as a close packed film embedded in a polymeric matrix (Figure 4d). Argon sputtering was used to etch both the polymeric matrix as well as the silica nanospheres to half their thickness. Then, the silica spheres were removed in HF leaving a porous nanopattern in the polymeric matrix. The nanopattern was then transferred by an oxygen plasma etch into an underlying film of polyethersulfone (PES). The described process was carried out on a silicon wafer coated with cellulose acetate (CA) as a sacrificial layer for membrane release; after membrane fabrication the CA was easily dissolved in acetone. The obtained PES nanoporous membrane exhibited 230 nm pores with a thickness of 500 nm.

Since characteristics such as size, ordering, and spacing of the deposited nanospheres directly determine the pore size and distribution of the resulting membrane, several groups have studied the role of the deposition processes. Jian-Hong Lee *et al.* [65], followed the evolution of a metallic mask deposited on PS spheres and found the PS spheres to move as a result of metallic growth underneath, eventually resulting in a continuous metallic layer rather than a nanostructured layer. This finding offers a simple parameter that can be used to obtain a feature size smaller than the spheres used. The use of isotropic plasma etching achieves sphere size reduction and consequently smaller feature size than the starting spheres; RIE is usually employed for this purpose. However, a combination of RIE-ICP (inductively coupled plasma) has shown to decrease the etch rates offering a closer control on the sphere shrinking process.[64] Jie Yu *et al.* [66], fabricated silver nanoparticles by depositing a thin layer of silver over close packed PS spheres. The nanoparticles exhibited sizes small as 50 nm. This method can be applied as a way to obtain secondary nanospheres of much smaller size. Furthermore, nanosphere assembly at the liquid-liquid interface has also been reported to yield non-close packed arrangement in which the spacing is easily tuned by setting the interface area constant while varying the number of particles introduced for self-assembly [67]. NSL is a versatile process used to fabricate nanostructured materials for a wide variety of applications.

5. Anodization

As fabrication has moved from the micro into the nanoscale, special interest has been given to spontaneous fabrication methods that yield nanostructured materials; naturally, anodization has come into play. In addition to commonly used Al, other anodized materials include Ti [68–72]; Ta [73]; Zr [74]; Nb [75]; GaN [76]; and have been studied for applications such as drug release [77], electrically active membranes [68], solar cells [71], and protein-releasing conductive membranes [78], among many others.

Anodization is a spontaneous process that oxidizes a material while creating cylindrical nanopores parallel to each other and perpendicular to their underlying metallic substrate [36]. The layer anodized during the initial step is allowed to reach symmetry and then

dissolved, leaving ordered concave pits in the substrate which serve as nucleation sites during the second anodization step [39]. The anodized aluminum oxide (AAO) layer presents open nanopores on one side and closed bottoms on the interface with the metallic substrate. This interface is referred to as the barrier layer and its chemical composition is the same as the AAO. When applied to membrane fabrication, the barrier layer and the metallic substrate can be dissolved to release a nanoporous AAO membrane [36].

One key characteristic of the anodization process is the achievement of very high aspect ratios of pore size to thickness while maintaining vertical sidewalls and periodic order [40]. Anodized materials have been widely employed because of their high aspect ratios; however, their very thick nature limit them to low transport rates [52]. More recently, increasing interest over small aspect ratios has emerged because of the mass transport advantages it offers. The latter expands the reach of anodized materials and calls for further research and development.

Successful preparation of anodized titanium oxide (ATO) from a Ti foil, followed by transfer from the foil to a foreign substrate has been reported by Lv *et al.* [69] (Figure 5a). After anodization, the ATO/Ti foil is immersed in water to undergo detachment. The authors believe that hydrogen trapped under the barrier layer further develops H_2 bubbles allowing water to penetrate this interface, releasing the H_2 present and resulting in complete membrane detachment. The ATO released membrane of 539 nm thickness with 115 nm pores achieved in this work as an efficient and low-cost alternative to electrodes for photoelectrochemical applications. Furthermore, this fabrication process exhibits great potential to apply ATO as separation media since it successfully produces a released nanoporous membrane that can be transferred onto a supporting frame and be used for separation strategies.

Yanagishita *et al.* [79], employed a two-step anodization process to fabricate a free-standing porous alumina membrane. Anodization was carried out in $H_2C_2O_4$ and H_2SO_4 for the first and second step, respectively. First anodization creates a highly soluble alumina layer selectively dissolved in a mixed solution of CrO_3 and H_3PO_4 which detaches the second alumina layer without pore widening. Although high aspect ratio AAO membranes were fabricated in this study, it is a promising approach for membrane detachment that can be readily applied to thinner AAO films.

Wen-Jeng Ho *et al.* [45], fabricated AAO from an Al foil which, after anodization, was immersed in a solution containing $CuCl_2$, HCl, and H_2O to etch the remaining Al foil (Figure 5b). They then used H_3PO_4 to remove the back barrier layer to fully open the pores. The process resulted in a free standing AAO ultrathin film with a pore diameter of 80 – 100 nm and a thickness of 190 nm. The ultrathin AAO was used as a template for the growth of silver nanoparticles. Although AAO is a strong material that becomes brittle over ultrathin sections with high porosity [39], the authors reported that the released ultrathin AAO did not break. SEM micrographs show a top view and cross-section of the though-pores in the AAO membrane after removal of the back barrier layer. Although free-standing ultrathin AAO membranes have been reported to be susceptible to splitting [80], this work successfully achieves an ultrathin free-standing AAO membrane stable enough to be transferred to

another substrate. This demonstrates the potential of AAO based materials as ultrafiltration membranes after optimizing its porous and mechanical properties.

Anodization most commonly uses very thick layers or foils of a metal as starting material, which sets a trade-off between thickness and stability. Mechanically stable anodized membranes are usually thick [81,82],[68,70,71,74,76] resulting in very high aspect ratios that significantly compromise on efficient mass flow across the membrane, hindering its potential as separation media. The successful anodization of metallic films deposited on Si wafers [72,83–85] and even glass [86] has been reported, which increases the versatility of anodized materials since it expands the processing catalog to conventional silicon technologies. The fabrication process reported by Okada *et al.* [72], accomplished complete anodization of the Ti layer yielding a membrane with a thickness of 80 nm with 30 nm pores. The thickness of the anodized titanium oxide (ATO) could be adjusted by changing the starting Ti deposited thickness to minimize the aspect ratio. Moreover, the fact that the ATO grows on a Si wafer offers the possibility of using DRIE or KOH bath to remove the back of the wafer and produce an ultrathin and free-standing ATO membrane. The latter approach was investigated by Wolfrum *et al.* [87]. The authors produced free-standing AAO membranes at the top of the truncated square pyramids. The publications reviewed in this section showcase the great potential of anodized based membranes.

6. Nanoimprint lithography

Nanoimprint lithography is a relatively new fabrication technique enabling patterning at the nanoscale with high throughput at a reasonable cost [42]. It requires thermoplastic materials such as PMMA to be heated above its glass transition temperature while being pushed into a mold. The polymer is cooled down after filling the mold retaining the developed shape. This process is also referred to as hot embossing. A variation of this process is the use of UV light to cure the material instead of cooling it, allowing for a low working pressure. Step or flash imprint lithography is performed with the lowest working pressure. A monomer solution is dispensed in droplets and then allowed to cure [43]. Nanoimprint lithography offers a wide variety of patterning processes such as lift-off, direct nanoimprint, stamping, transfer, stripping, and reversal [41].

Nanoimprint technologies are occasionally classified as expensive since the nanostructured master molds used are commonly fabricated through costly techniques such as e-beam lithography. This significantly increases the budget of research and development, since the master mold can only cover a small area and the patterns cannot be easily modified. Nevertheless, reported works have demonstrated the feasibility of using nanoimprint technologies for the fabrication of nanoporous membranes. Sainiemi *et al.* [89], fabricated silicon nanoporous membranes by UV-assisted nanoimprint lithography. The master mold presented circular patterns with a diameter of 300 nm, fabricated by e-beam lithography, from which a PDMS stamp was made. More recently, Nabar *et al.* [90] demonstrated the fabrication of Si_3N_4 nanoporous membranes through a thermal nanoimprint process. In their work, a commercially available silicon master mold presenting nanopillars with a diameter of 200 nm was used to imprint a photoresist pattern on a Si_3N_4 layer. The resulting membrane exhibited 385 nm pores with a thickness of 1 μm. The authors studied the

occurrence of defect events, namely connected and malformed pores and found the wafer average % of damaged pores to be 13.81% when evaluated on a single wafer over a 10x10 μm area.

Wong *et al.* [22] recently reported a strategy to tune pore thickness and diameter by utilizing a PDMS mold to imprint a nanoporous pattern on a polymeric film using capillary force driven mold-based lithography (Figure 6a). The PDMS master mold is brought in contact with the polymeric layer to produce pores exhibiting oval, circular or rod shapes with a pore size ranging from 80 to 400 nm; by controlling imprinting time and temperature. The fabrication technique reported includes the use of a sacrificial layer of poly(sodium 4-styrenesulfonate) (PSS) which is dissolved in water to mediate the release of the membrane. This simple nanoimprint fabrication process successfully expands the versatility of a single master mold to be used for the fabrication of membranes with a wide range of pore dimensions.

Furthermore, the ever increasing catalog of nanofabrication techniques has allowed the cost reduction of nanoimprint master molds as well. Several authors have reported the use of AAO for the fabrication of nanoimprint master molds. To the best of our knowledge, this alternative route has been rarely used to fabricate nanoporous films applied as membranes; however, it has been used for the fabrication of nanostructured materials for other applications that require a porous surface which illustrates its promising potential for the fabrication of nanoporous membranes.

The use of AAO templates hot-pressed against a polymeric or platinum-based metallic alloy to create a master mold of nanorods has been reported by Jianjun Li *et al.* [88] (Figure 6b). The obtained nanorods were subsequently used to produce nanopore arrays on a resist layer by hot embossing. The nanoporous resist film corresponding to SU-8 exhibited 207 nm pores with a thickness of 300 nm, fabricated from a PMMA-based master mold. Moreover, the AAO template has been used as a nanoimprint master mold itself [91].

Nanoimprint lithography has also been used to enable the fabrication of AAO with different morphologies, where the porous pattern is duplicated or even triplicated. The latter was achieved by nanoindentations on a PMMA layer through the use of a nanoimprint stamp, which was found to be closely correlated to the morphology of the AAO obtained [92]. Furthermore, the shape of the pore faces can also be controlled as reported by Masuda *et al.* [93], through the use of a SiC nanoimprint mold to produce square or triangular nanoindentations from which the anodization process develops to form square or triangular pore faces. Additionally, a mild-hard cyclic anodization has been shown to produce pores where the diameter fluctuates with depth [94]. These technique demonstrate the versatility of the well-known anodization process, expanding the catalog of AAO based nanoimprint master molds that can be produced.

One of the challenges of nanoimprint lithography is the correct alignment of the template and substrate, which if not done with precision can result in misalignment of the subsequent layers [42]. However, the fabrication of nanoporous membranes usually requires a single step of nanopatterning, hence the overlay is not a limiting factor. Furthermore, nanoimprint

lithography is a great candidate for scalable nanomanufacturing, by potentially enabling roll-to-roll processes. Master molds can be fabricated as spinning rods that when in contact with a moving substrate can imprint a pattern [41]. Roll-to-roll processes are highly desirable for mass manufacture because of significantly reduced costs.

7. Other applied or promising techniques

Other innovative mechanisms have also been studied with the goal of creating ultrathin membranes. Solid phase crystallization is a spontaneous phenomenon driven by the thermodynamics of materials crystallization which has been integrated into nanofabrication processes through similar pathways to produce free-standing nanoporous membranes. Similarly to NSL, lens lithography utilizes spherical beads to focus UV light and expose a nanoscale area on a photoresist layer. The well-known Stöber process offers a promising technique to produce nanoporous membranes through an approach very similar to self-organizing polymers. Furthermore, the self-assembly of molecules or nanoparticles has been reported for the fabrication of nanoporous membrane. Additionally, carbon nanotubes embedded in a matrix have been used as a nanoporous membrane and carbon nanotube removal from the matrix is another promising nanofabrication approach. Lastly, metal-assisted chemical etching is a promising tool to produce nanopores by etching a layer through the use of nanoparticles. These applied or promising techniques are discussed in this section.

Solid phase crystallization

Our collaborative teams have been researching the fabrication and application of ultrathin silicon-based porous membranes for over ten years. Striemer *et al.* [4], designed an innovative fabrication process driven by the spontaneous formation of voids in ultrathin silicon films due to solid phase crystallization (Figure 7a). The process requires the deposition of a three layer stack consisting of SiO_2/amorphous-Si/SiO_2 which undergoes a rapid thermal treatment to develop nanopores. The nanoporous silicon films were accessed by etching the back of the silicon wafer resulting in free-standing nanoporous membranes exhibiting pore sizes from 9 to 35 nm with a thickness of 15 nm. Parameters related to film deposition and thermal treatment were found to influence the pore size and distribution [105]. Membranes with pore diameters between 5 and 55 nm with 0.5 to 6.6% porosities and even >20% have been achieved by replacing SiO_2 with Si_3N_4 [106]. This fabrication method allows for carbonization as a post-fabrication means of controllably reducing the pore size by 1 to 25 nm. Moreover, the thin carbon coat further improves the chemical stability to alkaline solutions that rapidly etch silicon otherwise [107]. The nanoporous silicon membrane described has also been used as an etch mask to produce large-scale SiN membranes [108], which have been successfully released through wet and dry lift-off techniques [109]. The scale-up capability of this fabrication process has enabled us to consistently deliver nanoporous membranes with larger active area and improved mechanical stability while remaining ultrathin.

Another successful fabrication process was reported by Liu *et al.* [110], utilizing the self-assembly of cesium chloride (CsCl) islands. In this case, a CsCl layer was evaporated on a

sacrificial layer of polydimethyl glutarimide (PMGI); the samples underwent moisture exposure to promote the formation of islands. The obtained pattern was transferred into the PGMI film and reversed to form a chromium etch mask. The pattern was transferred into the Si_3N_4 layer and the produced membrane was accessed by etching the back of the silicon wafer. The obtained free-standing Si_3N_4 membranes exhibited pores in the range from 80 to 200 nm with a thickness of 200 nm. It has been reported that size and interpore spacing can be controlled by changing processing parameters such as CsCl thickness, relative humidity, exposure time, and temperature [111,112].

Nanosphere lens lithography

This is a maskless patterning process that enables the fabrication of nanopores or nanopillars through the use of conventional photolithography tools; using UV light focused by PS or silica nanospheres [113]. Wu *et al.* [114], reported the successful patterning of positive and negative photoresists through this approach, obtaining nanopores or nanopillars with a diameter between 500 and 700 nm by adjusting the exposure time through an assembled monolayer of 0.97 μm spheres (Figure 7b). Moreover, the lattice period was increased from 500 to 4000 nm through the use of larger nanospheres without impacting the size of the pores, due to the fact that the focused area is a very weak function of the sphere size. Feature sizes with a diameter of 180 nm and sexfoil-shaped features have been obtained through process optimization [104], [115]. Furthermore, feature size down to 75 nm has been obtained by using an interlayer of silver to enhance the evanescent wave by surface plasmon excitation [116]. Although, more research needs to be done to explore its reach, lens lithography stands as a straightforward technique that can be readily applied to membrane fabrication.

Stöber-process

The Stöber process is an example of a sol-gel method through which molecules from a precursor reorganize in solution to form new structures; it remains as a commonly used process for the production of silica nanostructures since it was first reported by Werner Stöber in 1968 [117]. Porous silica films can be produced by the addition of a surfactant to promote initial micellar formation that evolves into well-aligned pores.

Zhaogang Teng *et al.* [53], reported the successful formation of mesoporous silica films formed on silicon with aligned pores of 2.3 nm average size. Film thickness was varied from 34 to 240 nm when adjusting the water/ethanol or precursor/surfactant ratio and deposition time. The use of similar porous silica films as separation media was reported by Lin *et al.* [118]. In their work, the porous silica film was synthesized on an ITO substrate and then transferred to a microporous Si_3N_4 membrane supported on a silicon wafer. Thickness was controlled by adjusting the deposition time between 4 and 24 h to yield a final thickness of 14 to 118 nm. Produced porous silica of all thicknesses were successfully transferred without breaking or wrinkling.

The Stöber process offers a simple approach to obtain quality porous silica that can be transferred to a foreign substrate and has already been applied for molecular separation

based on size and charge [13]. Variation of pore size may be attained through the use of different surfactants that create larger micelles; however, this remains a subject to be studied.

Metal-assisted chemical etching

The use of metallic nanoparticles in etching solutions has been implemented as a simple method for the production of morphologies of nanopillars or nanopores. Zhu *et al.* [119], utilized a colloidal gold solution in HF/H_2O_2 to produce random porous structures (20 nm wide) on the surface of a silicon wafer where the pores followed the <100> planes when propagating below the surface. More recently, an array of gold nanoparticles was employed for the fabrication of nanowires and nanopillars [120]. A similar approach utilizes gold nanoparticles heated close to their melting point, promoting their diffusion perpendicularly into amorphous substrates such as SiO_2 and Si_3N_4. De Vreede *et al.* [121] found that under optimized conditions, nanoparticle diffusion leaves nanopores 25 nm wide. Additional research and development of this process should be done since it represents a valuable tool that can be integrated into a nanofabrication process for the creation of pores.

Membranes based on the assembly of nanoparticles/molecules

Protein-based membranes have achieved very small pore sizes through simple assembly processes. These membranes are formed by proteins such as ferritin that assemble around metal hydroxide nanostrands which are then removed; the protein film is crosslinked to yield a robust membrane, although the pores formed are not always through-pores. Peng *et al.* [122], reported the fabrication of a ferritin membrane exhibiting 2.2 nm pores in a 60 nm thick membrane. Van Rijn *et al.* [123], reported another ferritin-based membrane; however, in their work the protein is embedded in a polymer matrix assembled at an air/water interface. The ferritin is then denaturized, leaving a polymeric nanoporous 7 nm thick membrane exhibiting pores with selectivity to particles below 20 nm. Similarly, dodecanethiol-ligated gold nanocrystals were reported by He *et al.* [124], to assemble at a water/air interface to form a thin nanoporous film after drying. These membranes consisted of four layers sequentially deposited to a final thickness of 34 nm; hence, a 100% population of through-pores is not expected. The obtained membrane exhibited >99% rejection of nanoparticles with a diameter ≥ 2nm. Although membranes presenting through pores remain to be obtained, this approach shows future promise.

Carbon based membranes

Carbon nanotube (CNT) based membranes have also been investigated since very small diameters can be achieved. Hinds *et al.* [125], fabricated an array of aligned CNT embedded in a polymeric matrix and released from the quartz substrate in HF leaving the CNT tips opened. The resulting membrane exhibited 7.5 nm pores with a thickness of 5 to 10 μm. Moreover, functionalizing the open ends of the CNT allows controlled chemical or ionic separations. Although these membranes are very thick, gas and liquid transport show a 15 – 30 and 1000 – 10 000 fold increase from the values predicted by Knudsen diffusion and no slip hydrodynamic calculations respectively [126].

Holt *et al.* [127], reported the fabrication of a CNT-based membrane grown on a silicon substrate with iron as a catalyst. SiN_x was then deposited to fill in the bulk of the CNT

without losing alignment. The membrane was accessed by wet etch removal of exposed silicon on the back of the wafer. This CNT membrane exhibited a lower molar flux than predicted due to the bamboo morphology. Additionally, the CNTs were removed through an oxidation process leaving a SiN_x nanoporous membrane; exhibiting an estimated average pore size of 66 nm. Nanofabrication involving CNT remains an interesting approach to achieve very small pores; however, further investigation and development need to be done in order to achieve a CNT morphology free of defects that hinder mass flow.

Graphene membranes have also been fabricated by treating graphene layers with an oxygen plasma producing nanopores exhibiting a diameter of 1 nm as reported by Surwade *et al.* [128]. The pore formation could be tracked by Raman spectroscopy by evaluating the intensity ratio and shape of the D and G peaks. Similarly, introduction of defects by ionic bombardment causes the formation of pores which can be further enlarged through etching to form pores with diameters of <1 nm. Pore density reaches a maximum equivalent to ionic bombardment density, suggesting each ion acting as a seed from which a single pore is created [129]. Graphene based membranes provide an aspect ratio close to one for very small pore sizes (≤1 nn), hence are of great interest for the separation of very small molecules.

Controlled breakdown

Another promising technique for the fabrication of nanopores of <2 nm in size takes advantage of the dielectric breakdown of thin films when exposed to high electric fields. The successful formation of single nanopores has been demonstrated by Briggs *et al.* [130], in Si_3N_4 films in the presence of aqueous and organic environments. The main interest in single nanopore membranes derives from their potential application as DNA analysis and sequencing platforms.

8. Conclusions

Advancement of nanofabrication techniques continues to enable the production of nanostructured materials in many areas of science and for a wide range of applications. The techniques reviewed here correspond to processes yielding through-pore nanoporous membranes with a pore size to thickness ratio close to one, ensuring efficient mass transport due to improved selectivity and high permeability. These membranes have been fabricated thorough large-area and low-cost methods that are inherently scalable to large scale manufacturing. Most separation applications can tolerate some variation in pore size and distribution. The most common point defects found during membrane fabrication are related to the absence of pores or variation of pore size. The former is not significant for ultrafiltration strategies and the latter can be optimized to ensure membrane functionality and optimal efficiency. The nanofabrication techniques reviewed show great versatility and can be utilized for organic and inorganic materials to produce membranes exhibiting a wide range of geometries. These processes can be easily performed in research laboratories and integrated into more complex assemblies, showing great potential for a variety of applications, advancing many areas of research. The catalog of nanofabrication processes

will continue to expand and allow for increasingly sophisticated and reliable membranes applied in ultrafiltration technologies.

Acknowledgments

We thank the Rochester Nanomembrane Research Group (NRG) for their ideas and helpful comments. The authors declare the following competing financial interest: TRG is a co-founder of SiMPore, a nano materials start-up company that commercializes ultrathin membranes.

List of abbreviations

AAO	Anodized aluminum oxide
ATO	Anodized titanium oxide
BCP	Block copolymers
BOE	Buffered oxide etch
BSA	Bovine serum albumin
CA	Cellulose acetate
CNT	Carbon nanotube
CsCl	Cesium chloride
DRIE	Deep reactive ion etch
HF	Hydrofluoric acid
HRV14	Human rhinovirus type 14
ICP	Inductively coupled plasma
ITO	Indium tin oxide
KOH	Potassium hydroxide
NSL	Nanosphere lithography
P2VP	Poly(2-vinylpyridine
PEO	Polystyrene-block-poly(ethylene oxide)
PES	polyethersulfone
PHEMA	Poly(hydroxyethyl methacrylate)
PI	Poly(isoprene)
PLA	Poly(lactide)
PMGI	Polydimethyl glutarimide
PMMA	Poly (methyl methacrylate)

PS	Polystyrene
PSS	Poly(sodium 4-styrenesulfonate)
RIE	Reactive ion etch
SEM	Scanning electron microscope
Si_3N_4	Silicon nitride
SiO_2	Silicon oxide

References

1. Oyama, ST., Stagg-Williams, SM. Inorganic, Polymeric and Composite Membranes: Structure, Function and Other Correlations. Elsevier; 2011.
2. Zydney AL, Aimar P, Meireles M, et al. Use of the log-normal probability density function to analyze membrane pore size distributions: functional forms and discrepancies. J Memb Sci. 1994; 91(3):293–298.
3. Robertson BC, Zydney AL. Protein adsorption in asymmetric ultrafiltration membranes with highly constricted pores. J Colloid Interface Sci. 1990; 134(2):563–575.
4. Striemer CC, Gaborski TR, McGrath JL, Fauchet PM. Charge- and size-based separation of maeromolecules using novel ultrathin silicon membranes. Nature. 2007 Feb.445
5. Montagne F, Blondiaux N, Bojko A, Pugin R. Molecular transport through nanoporous silicon nitride membranes produced from self-assembling block copolymers. Nanoscale. 2012; 4(19):5880–6. [PubMed: 22899238]
6. Mehta A, Zydney AL. Permeability and selectivity analysis for ultrafiltration membranes. J Memb Sci. 2005; 249(1):245–249.
7. Apel PY, Blonskaya IV, Dmitriev SN, et al. Structure of polycarbonate track-etch membranes: Origin of the “paradoxical” pore shape. J Memb Sci. 2006; 282(1):393–400.
8. Gaborski TR, Snyder JL, Striemer CC, et al. High-Performance Separation of Nanoparticles with Ultrathin Porous Nanocrystalline Silicon Membranes. ACS Nano. 2010; 4(11):6973–6981. [PubMed: 21043434]
9. Smith KJP, Winans JD, McGrath JL. Silicon Nanomembranes for Efficient and Precise Molecular Separations. Silicon Nanomembranes Fundam Sci Appl. 2016
10. Snyder JL, Clark A, Fang DZ, et al. An experimental and theoretical analysis of molecular separations by diffusion through ultrathin nanoporous membranes. J Memb Sci. 2011; 369(1–2): 119–129. [PubMed: 21297879]
11. Johnson DG, Khire TS, Lyubarskaya YL, et al. Ultrathin silicon membranes for wearable dialysis. Adv Chronic Kidney Dis. 2013; 20(6):508–515. [PubMed: 24206603]
12. Burgin, T., Johnson, D., Chung, H., et al. Ultrathin Silicon Membranes for Improving Extracorporeal Blood Therapies. ASME 2016 14th Int. Conf. Nanochannels, Microchannels, Minichannels collocated with ASME 2016 Heat Transf. Summer Conf. ASME 2016 Fluids Eng. Div. Summer Meet; 2016. p. V001T15A003-V001T15A003.
13. Yang Q, Lin X, Su B. Molecular Filtration by Ultrathin and Highly Porous Silica Nanochannel Membranes: Permeability and Selectivity. Anal Chem. 2016 acs.analchem.6b02968.
14. Yang SY, Ryu I, Kim HY, et al. Nanoporous membranes with ultrahigh selectivity and flux for the filtration of viruses. Adv Mater. 2006; 18(6):709–712.
15. Biswas A, Bayer IS, Biris AS, et al. Advances in top-down and bottom-up surface nanofabrication: Techniques, applications & future prospects. Adv Colloid Interface Sci. 2012; 170(1–2):2–27. [PubMed: 22154364]
16. Cho HJ, Oh HS, Nam KJ, et al. Si FinFET based 10nm technology with multi Vt gate stack for low power and high performance applications. Dig Tech Pap - Symp VLSI Technol. 2016 2016–Septe, 12–13.

17. Mojarad N, Gobrecht J, Ekinci Y. Interference lithography at EUV and soft X-ray wavelengths: Principles, methods, and applications. Microelectron Eng. 2015; 143:55–63.
18. De Simone D, Goethals AM, Van Roey F, et al. Progresses and Challenges of EUV Lithography Materials. J Photopolym Sci Technol. 2014; 27(5):601–610.
19. Apel P. Track etching technique in membrane technology. Radiat Meas. 2001; 34(1–6):559–566.
20. Vlassiouk I, Apel PY, Dmitriev SN, et al. Versatile ultrathin nanoporous silicon nitride membranes. Proc Natl Acad Sci. 2009; 106(50):21039–21044. [PubMed: 19948951]
21. Han J, Fu J, Schoch RB. Molecular sieving using nanofilters: past, present and future. Lab Chip. 2008; 8(1):23–33. [PubMed: 18094759]
22. Wong HC, Zhang Y, Viasnoff V, Low HY. Predictive Design, Etch-Free Fabrication of Through-Hole Membrane with Ordered Pores and Hierarchical Layer Structure. Adv Mater Technol. 2017; 2(2):1600169.
23. Li W, Müller M. Directed self-assembly of block copolymers by chemical or topographical guiding patterns: Optimizing molecular architecture, thin-film properties, and kinetics. Prog Polym Sci. 2016; 54–55:47–75.
24. Ji S, Wan L, Liu CC, Nealey PF. Directed self-assembly of block copolymers on chemical patterns: A platform for nanofabrication. Prog Polym Sci. 2016; 54–55:76–127.
25. Wang Y, Li F. An emerging pore-making strategy: Confined swelling-induced pore generation in block copolymer materials. Adv Mater. 2011; 23(19):2134–2148. [PubMed: 21469216]
26. van Reis R, Zydney A. Bioprocess membrane technology. J Memb Sci. 2007; 297(1–2):16–50.
27. Li M, Ober CK. Block copolymer patterns and templates. Mater Today. 2006; 9(9):30–39.
28. Segalman RA. Patterning with block copolymer thin films. Mater Sci Eng R Reports. 2005; 48(6): 191–226.
29. Park C, Yoon J, Thomas EL. Enabling nanotechnology with self assembled block copolymer patterns. Polymer (Guildf). 2003; 44(22):6725–6760.
30. Vogel N, Retsch M, Fustin CA, et al. Advances in Colloidal Assembly: The Design of Structure and Hierarchy in Two and Three Dimensions. Chem Rev. 2015; 115(13):6265–6311. [PubMed: 26098223]
31. Ai B, Yu Y, M??hwald H, et al. Plasmonic films based on colloidal lithography. Adv Colloid Interface Sci. 2014; 206:5–16. [PubMed: 24321859]
32. Acikgoz C, Hempenius MA, Huskens J, Vancso GJ. Polymers in conventional and alternative lithography for the fabrication of nanostructures. Eur Polym J. 2011; 47(11):2033–2052.
33. Ye X, Qi L. Two-dimensionally patterned nanostructures based on monolayer colloidal crystals: Controllable fabrication, assembly, and applications. Nano Today. 2011; 6(6):608–631.
34. Yang SM, Jang SG, Choi DG, et al. Nanomachining by colloidal lithography. Small. 2006; 2(4): 458–475. [PubMed: 17193068]
35. Haynes C, Van Duyne R. Nanosphere Lithography: A Versatile Nanofabrication Tool for Studies of Size-Dependent Nanoparticle Optics. J Phys Chem B. 2001:5599–5611.
36. Mijangos C, Hernández R, Martín J. A review on the progress of polymer nanostructures with modulated morphologies and properties, using nanoporous AAO templates. Prog Polym Sci. 2016; 54–55:148–182.
37. Wang K, Liu G, Hoivik N, et al. Electrochemical engineering of hollow nanoarchitectures: pulse/step anodization (Si, Al, Ti) and their applications. Chem Soc Rev. 2014; 43(5):1476–500. [PubMed: 24292021]
38. Kowalski D, Kim D, Schmuki P. TiO2 nanotubes, nanochannels and mesosponge: Self-organized formation and applications. Nano Today. 2013; 8(3):235–264.
39. Ingham CJ, ter Maat J, de Vos WM. Where bio meets nano: The many uses for nanoporous aluminum oxide in biotechnology. Biotechnol Adv. 2012; 30(5):1089–1099. [PubMed: 21856400]
40. Chik H, Xu JM. Nanometric superlattices: Non-lithographic fabrication, materials, and prospects. Mater Sci Eng R Reports. 2004; 43(4):103–138.
41. Yu CC, Chen HL. Nanoimprint technology for patterning functional materials and its applications. Microelectron Eng. 2015; 132:98–119.

42. Lan H, Ding Y, Liu H, Lu B. Review of the wafer stage for nanoimprint lithography. Microelectron Eng. 2007; 84(4):684–688.
43. Truskett VN, Watts MPC. Trends in imprint lithography for biological applications. Trends Biotechnol. 2006; 24(7):312–317. [PubMed: 16759722]
44. Acikgoz C, Ling XY, Phang IY, et al. Fabrication of freestanding nanoporous polyethersulfone membranes using organometallic polymer resists patterned by nanosphere lithography. Adv Mater. 2009; 21(20):2064–2067.
45. Ho WJ, Cheng PY, Hsiao KY. Plasmonic silicon solar cell based on silver nanoparticles using ultra-thin anodic aluminum oxide template. Appl Surf Sci. 2015; 354:25–30.
46. Kutowy O, Thayer WL, Sourirajan S. High flux cellulose acetate ultrafiltration membranes. Desalination. 1978; 26(16877):195–210.
47. Altinpinar S, Zhao H, Ali W, et al. Distortion of Ultrathin Photocleavable Block Copolymer Films during Photocleavage and Nanopore Formation. Langmuir. 2015; 31(32):8947–8952. [PubMed: 26161944]
48. Bates FS, Fredrickson GH. Block copolymer thermodynamics: theory and experiment. Annu Rev Phys Chem. 1990; 41(1):525–557. [PubMed: 20462355]
49. Schumers JM, Vlad A, Huynen I, et al. Functionalized nanoporous thin films from photocleavable block copolymers. Macromol Rapid Commun. 2012; 33(3):199–205. [PubMed: 22184052]
50. Yang SY, Park J, Yoon J, et al. Virus filtration membranes prepared from nanoporous block copolymers with good dimensional stability under high pressures and excellent solvent resistance. Adv Funct Mater. 2008; 18(9):1371–1377.
51. Nuxoll EE, Hillmyer MA, Wang R, et al. Composite block polymer-microfabricated silicon nanoporous membrane. ACS Appl Mater Interfaces. 2009; 1(4):888–893. [PubMed: 20160882]
52. Popa AM, Niedermann P, Heinzelmann H, et al. Fabrication of nanopore arrays and ultrathin silicon nitride membranes by block-copolymer-assisted lithography. Nanotechnology. 2009; 20(48):485303. [PubMed: 19880976]
53. Teng Z, Zheng G, Dou Y, et al. Highly ordered mesoporous silica films with perpendicular mesochannels by a simple st??ber-solution growth approach. Angew Chemie - Int Ed. 2012; 51(9): 2173–2177.
54. Kim SH, Misner MJ, Xu T, et al. Highly oriented and ordered arrays from block copolymers via solvent evaporation. Adv Mater. 2004; 16(3):226–231.
55. Xu T, Zhu Y, Gido SP, Russell TP. Electric Field Alignment of Symmetric Diblock Copolymer Thin Films. Macromolecules. 2004; 37(7):2625–2629.
56. Tang YH, Huang MJ, Shiao MH, Yang CR. Fabrication of silicon nanopillar arrays and application on direct methanol fuel cell. Microelectron Eng. 2011; 88(8):2580–2583.
57. Wu HC, Bao MD, Ma KJ, Chien HH. Fabrication of size-tunable Cr nanodots and nanorings array by modified nanosphere lithography. Micro Nano Lett. 2012; 7(10):1056–1059.
58. Lotito V, Zambelli T. Self-assembly and nanosphere lithography for large-area plasmonic patterns on graphene. J Colloid Interface Sci. 2015; 447:202–210. [PubMed: 25432446]
59. Purwidyantri A, Chen CH, Hwang BJ, et al. Spin-coated Au-nanohole arrays engineered by nanosphere lithography for a Staphylococcus aureus 16S rRNA electrochemical sensor. Biosens Bioelectron. 2016; 77:1086–1094. [PubMed: 26556186]
60. Kang C, Ramakrishna SN, Nelson A, et al. Ultrathin, freestanding, stimuli-responsive, porous membranes from polymer hydrogel-brushes. Nanoscale. 2015; 7(30):13017–13025. [PubMed: 26169114]
61. Klein MJK, Montagne F, Blondiaux N, et al. SiN membranes with submicrometer hole arrays patterned by wafer-scale nanosphere lithographya) SiN membrane masks for x-ray lithography SiN membranes with submicrometer hole arrays patterned by wafer-scale nanosphere lithography. J Vac Sci Technol B J Appl Phys Phys Lett J Vac Sci Technol. 2011; 29(20):21012–2599.
62. Lipson AL, Comstock DJ, Hersam MC. Nanoporous templates and membranes formed by nanosphere lithography and aluminum anodization. Small. 2009; 5(24):2807–2811. [PubMed: 19859942]
63. Muñoz-Espí R, Weiss CK, Landfester K. Inorganic nanoparticles prepared in miniemulsion. Curr Opin Colloid Interface Sci. 2012; 17(4):212–224.

64. Plettl A, Enderle F, Saitner M, et al. Non-Close-Packed crystals from self-assembled polystyrene spheres by isotropic plasma etching: adding flexibility to colloid lithography. Adv Funct Mater. 2009; 19(20):3279–3284.

65. Lee JH, Chung YW, Hon MH, Leu IC. Fabrication of tunable pore size of nickel membranes by electrodeposition on colloidal monolayer template. J Alloys Compd. 2011; 509(23):6528–6531.

66. Yu, Jie, Geng, Chong, Zheng, Lu, Ma, Zhaohui, Tan, Tianya, Wang, Xiaoqing, Yan, Qingfeng, Shen, Dezhong. Preparation of High-Quality Colloidal Mask for Nanosphere Assembly and Solvent Vapor Annealing Preparation of High-Quality Colloidal Mask for Nanosphere Lithography by a Combination of Air / Water Interface Self- Assembly and Solvent Vapor Annealing. Langmuir. 2012; 28:12681– 12689. [PubMed: 22894745]

67. Isa L, Kumar K, Müller M, et al. Particle lithography from colloidal self-assembly at liquid-liquid interfaces. ACS Nano. 2010; 4(10):5665–5670. [PubMed: 20931974]

68. Albu SP, Ghicov A, Berger S, et al. TiO2 nanotube layers: Flexible and electrically active flow-through membranes. Electrochem commun. 2010; 12(10):1352–1355.

69. Lv H, Li N, Zhang H, et al. Transferable TiO2 nanotubes membranes formed via anodization and their application in transparent electrochromism. Sol Energy Mater Sol Cells. 2016; 150:57–64.

70. Barthwal S, Kim YS, Lim SH. Fabrication of amphiphobic surface by using titanium anodization for large-area three-dimensional substrates. J Colloid Interface Sci. 2013; 400:123–129. [PubMed: 23545242]

71. Mohammadpour F, Moradi M. Double-layer TiO_2 nanotube arrays by two-step anodization: Used in back and front-side illuminated dye-sensitized solar cells. Mater Sci Semicond Process. 2015; 39:255–264.

72. Okada M, Tajima K, Yamada Y, Yoshimura K. Self-Organized Formation of Short TiO2 Nanotube Arrays By Complete Anodization of Ti Thin Films. Phys Procedia. 2012; 32:714–718.

73. Horwood CA, El-Sayed HA, Birss VI. Precise electrochemical prediction of short tantalum oxide nanotube length. Electrochim Acta. 2014; 132:91–97.

74. Fang D, Liu S, Luo Z, et al. Facile fabrication of freestanding through-hole ZrO 2 nanotube membranes via two-step anodization methods. Appl Surf Sci. 2012; 258(17):6217–6223.

75. Choi J, Lim JH, Lee SC, et al. Porous niobium oxide films prepared by anodization in HF/H3PO4. Electrochim Acta. 2006; 51(25):5502–5507.

76. Schwab MJ, Chen D, Han J, Pfefferle LD. Aligned mesopore arrays in GaN by anodic etching and photoelectrochemical surface etching. J Phys Chem C. 2013; 117(33):16890–16895.

77. Jeon G, Yang SY, Byun J, Kim JK. Electrically actuatable smart nanoporous membrane for pulsatile drug release. Nano Lett. 2011; 11(3):1284–1288. [PubMed: 21280644]

78. Altuntas S, Buyukserin F, Haider A, et al. Protein-releasing conductive anodized alumina membranes for nerve-interface materials. Mater Sci Eng C. 2016; 67:590–598.

79. Yanagishita T, Masuda H. High-Throughput Fabrication Process for Highly Ordered Through-Hole Porous Alumina Membranes Using Two-Layer Anodization. Electrochim Acta. 2015; 184:80–85.

80. Lei Y, Chim W, VED. Shape and Size Control of Regularly Arrayed Nanodots Fabricated Using Ultrathin Alumina Masks. 2005; (26):580–585.

81. Akiya S, Kikuchi T, Natsui S, et al. Self-ordered Porous Alumina Fabricated via Phosphonic Acid Anodizing. Electrochim Acta. 2016; 190:471–479.

82. Zaraska L, Sulka GD, Szeremeta J, Jaskuła M. Porous anodic alumina formed by anodization of aluminum alloy (AA1050) and high purity aluminum. Electrochim Acta. 2010; 55(14):4377–4386.

83. Wang C, Cho SJ, Kim NY. High-luminance and high-efficiency multi-chip light-emitting diode array packaging platform with nanoscale anodized aluminum oxide on silicon substrate. Thin Solid Films. 2014; 557:346–350.

84. Jung YW, Byun JS, Woo DH, Kim YD. Ellipsometric analysis of porous anodized aluminum oxide films. Thin Solid Films. 2009; 517(13):3726–3730.

85. Ortiz GF, Hanzu I, Knauth P, et al. TiO2 nanotubes manufactured by anodization of Ti thin films for on-chip Li-ion 2D microbatteries. Electrochim Acta. 2009; 54(17):4262–4268.

86. Kilinç N, Şennik E, Öztürk ZZ. Fabrication of TiO2 nanotubes by anodization of Ti thin films for VOC sensing. Thin Solid Films. 2011; 520(3):953–958.

87. Wolfrum B, Mourzina Y, Sommerhage F, Offenhäusser A. Suspended nanoporous membranes as interfaces for neuronal biohybrid systems. Nano Lett. 2006; 6(3):453–457. [PubMed: 16522041]
88. Li J, Zhang W, Song Y, et al. Template Transfer Nanoimprint for Uniform Nanopores and Nanopoles. J Nanomater. 2016; 2016
89. Sainiemi L, Viheriälä J, Sikanen T, et al. Nanoperforated silicon membranes fabricated by UV-nanoimprint lithography, deep reactive ion etching and atomic layer deposition. J Micromechanics Microengineering. 2010; 20(7):77001.
90. Nabar BP, Çelik-Butler Z, Dennis BH, Billo RE. A nanoporous silicon nitride membrane using a two-step lift-off pattern transfer with thermal nanoimprint lithography. J Micromechanics Microengineering. 2012; 22(4):45012.
91. Sun T, Xu Z, Zhao W, et al. Fabrication of the similar porous alumina silicon template for soft UV nanoimprint lithography. Appl Surf Sci. 2013; 276:363–368.
92. Noh K, Choi C, Kim JY, et al. Long-range ordered aluminum oxide nanotubes by nanoimprint-assisted aluminum film surface engineering. J Vac Sci Technol B Microelectron Nanom Struct. 2010; 28(6):C6M88.
93. Masuda H, Asoh H, Watanabe M, et al. Square and triangular nanohole array architectures in anodic alumina. Adv Mater. 2001; 13(3):189–192.
94. Lee W, Ji R, Gösele U, Nielsch K. Fast fabrication of long-range ordered porous alumina membranes by hard anodization. Nat Mater. 2006; 5(9):741–747. [PubMed: 16921361]
95. Jung YS, Ross CA. Orientation-controlled self-assembled nanolithography using a polystyrene - polydimethylsiloxane block copolymer. Nano Lett. 2007; 7(7):2046–2050. [PubMed: 17570733]
96. Cheng JY, Ross CA, Thomas EL, et al. Templated Self-Assembly of Block Copolymers: Effect of Substrate Topography. Adv Mater. 2003; 15(19):1599–1602.
97. Ormonde AD, Hicks ECM, Castillo J, Van Duyne RP. Nanosphere lithography: Fabrication of large-area Ag nanoparticle arrays by convective self-assembly and their characterization by scanning UV - Visible extinction spectroscopy. Langmuir. 2004; 20(16):6927–6931. [PubMed: 15274605]
98. Yu L, Chen B, Xiao JM. A scheme of reconstructing network attack path. Dianzi Keji Daxue Xuebao/Journal Univ Electron Sci Technol China. 2006; 35(3):392–395.
99. Sulka GD, Parkoła KG. Temperature influence on well-ordered nanopore structures grown by anodization of aluminium in sulphuric acid. Electrochim Acta. 2007; 52(5):1880–1888.
100. Li J, Zhang Z, Li Y, et al. Self-Organization Process of Aluminum Oxide during Hard Anodization. Electrochim Acta. 2016; 213:14–20.
101. Chen L, Deng X, Wang J, et al. Defect control in nanoimprint lithography. J Vac Sci Technol B. 2005; 23(6):2933–2938.
102. Hirai Y, Yoshida S, Takagi N. Defect analysis in thermal nanoimprint lithography. J Vac Sci Technol B. 2003; 21(6):2765–2770.
103. Zhou W, Niu X, Min G, et al. Porous alumina nano-membranes: Soft replica molding for large area UV-nanoimprint lithography. Microelectron Eng. 2009; 86(12):2375–2380.
104. Wu W, Dey D, Katsnelson A, et al. Large areas of periodic nanoholes perforated in multistacked films produced by lift-off. J Vac Sci Technol B Microelectron Nanom Struct. 2008; 26(5):1745.
105. Fang DZ, Striemer CC, Gaborski TR, et al. Methods for controlling the pore properties of ultra-thin nanocrystalline silicon membranes. J Phys Condens Matter. 2010; 22(45):454134. [PubMed: 21339620]
106. Qi C, Striemer CC, Gaborski TR, et al. Highly porous silicon membranes fabricated from silicon nitride/silicon stacks. Small. 2014; 10(14):2946–2953. [PubMed: 24623562]
107. Fang DZ, Striemer CC, Gaborski TR, et al. Pore size control of ultrathin silicon membranes by rapid thermal carbonization. Nano Lett. 2010; 10(10):3904–3908. [PubMed: 20839831]
108. DesOrmeaux JPS, Winans JD, Wayson SE, et al. Nanoporous silicon nitride membranes fabricated from porous nanocrystalline silicon templates. Nanoscale. 2014; 6(18):10798. [PubMed: 25105590]
109. Miller JJ, Carter RN, McNabb KB, et al. Lift-off of large-scale ultrathin nanomembranes. J Micromechanics Microengineering. 2015; 25(1):15011.

110. Liu W, Ferguson M, Yavuz M, Cui B. Porous TEM windows fabrication using CsCl self-assembly. J Vac Sci Technol B Microelectron Nanom Struct. 2012; 201(2012)
111. Green M, Tsuchiya S. Mesoscopic hemisphere arrays for use as resist in solid state structure fabrication. J Vac Sci Technol B Microelectron Nanom Struct. 1999; 17:2074.
112. Liao YX, Liu J, Wang B, Yi FT. Nanopillars by cesium chloride self-assembly and dry etching. Mater Lett. 2012; 67(1):323–325.
113. Zhang Z, Geng C, Hao Z, et al. Recent advancement on micro-/nano-spherical lens photolithography based on monolayer colloidal crystals. Adv Colloid Interface Sci. 2016; 228:105–122. [PubMed: 26732300]
114. Wu W, Katsnelson A, Memis OG, Mohseni H. A deep sub-wavelength process for the formation of highly uniform arrays of nanoholes and nanopillars. Nanotechnology. 2007
115. Geng C, Yan Q, Du C, et al. Large-Area and Ordered Sexfoil Pore Arrays by Spherical-Lens Photolithography. ACS Photonics. 2014; 1(8):754–760.
116. Li S, Du C, Dong X, et al. Superlens nano-patterning technology based on the distributed Polystyrene spheres. Opt Express. 2008; 16(19):14397. [PubMed: 18794975]
117. Stöber W, Fink A, Bohn E. Controlled growth of monodisperse silica spheres in the micron size range. J Colloid Interface Sci. 1968; 26(1):62–69.
118. Lin X, Yang Q, Ding L, Su B. Ultrathin Silica Membranes with Highly Ordered and Perpendicular Nanochannels for Precise and Fast Molecular Separation. ACS Nano. 2015; 9(11): 11266–11277. [PubMed: 26458217]
119. Zhu J, Bart-Smith H, Begley MR, et al. Formation of Silicon Nanoporous Structures Induced by Colloidal Gold Nanoparticles in HF/H 2 O 2 Solutions. Chem Mater. 2009; 21(13):2721–2726.
120. Elnathan R, Isa L, Brodoceanu D, et al. Versatile Particle-Based Route to Engineer Vertically Aligned Silicon Nanowire Arrays and Nanoscale Pores. ACS Appl Mater Interfaces. 2015; 7(42): 23717–23724. [PubMed: 26428032]
121. De Vreede LJ, Van Den Berg A, Eijkel JCT. Nanopore fabrication by heating au particles on ceramic substrates. Nano Lett. 2015; 15(1):727–731. [PubMed: 25548953]
122. Peng X, Jin J, Nakamura Y, et al. Ultrafast permeation of water through protein-based membranes. Nat Nanotechnol. 2009; 4(6):353–357. [PubMed: 19498395]
123. Van Rijn P, Tutus M, Kathrein C, et al. Ultra-thin self-assembled protein-polymer membranes: A new pore forming strategy. Adv Funct Mater. 2014; 24(43):6762–6770.
124. He J, Lin XM, Chan H, et al. Diffusion and filtration properties of self-assembled gold nanocrystal membranes. Nano Lett. 2011; 11(6):2430–2435. [PubMed: 21548617]
125. Hinds BJ, Chopra N, Rantell T, et al. Aligned multiwalled carbon nanotube membranes. Science. 2004; 303(5654):62–65. [PubMed: 14645855]
126. Majumder M, Chopra N, Hinds BJ. Mass Transport through Carbon Nanotube Membranes in Three Di ff erent Regimes: Ionic Di ff usion and Gas and Liquid Flow. ACS Nano. 2011; 5:3867–3877. [PubMed: 21500837]
127. Holt JK, Noy A, Huser T, et al. Fabrication of a carbon nanotube-embedded silicon nitride membrane for studies of nanometer-scale mass transport. Nano Lett. 2004; 4(11):2245–2250.
128. Surwade SP, Smirnov SN, Vlassiouk IV, et al. Water desalination using nanoporous single-layer graphene. Nat Nanotechnol. 2015; 10(5):459–64. [PubMed: 25799521]
129. O'Hern SC, Boutilier MSH, Idrobo JC, et al. Selective ionic transport through tunable subnanometer pores in single-layer graphene membranes. Nano Lett. 2014; 14(3):1234–1241. [PubMed: 24490698]
130. Briggs K, Charron M, Kwok H, et al. Kinetics of nanopore fabrication during controlled breakdown of dielectric membranes in solution. Nanotechnology. 2015; 26(8):84004.

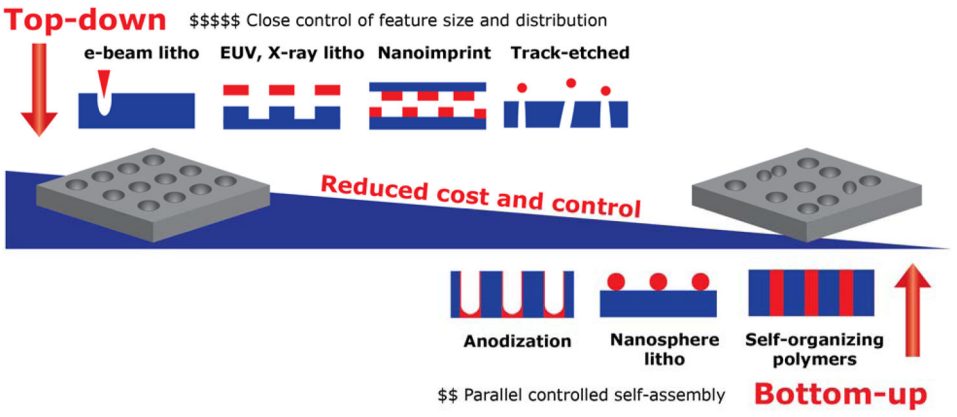

Figure 1.

Schematic comparison of top-down and bottom-up nanofabrication techniques used for the production of nanoporous membranes. Top-down methods offer closer control while bottom-up methods are inexpensive.

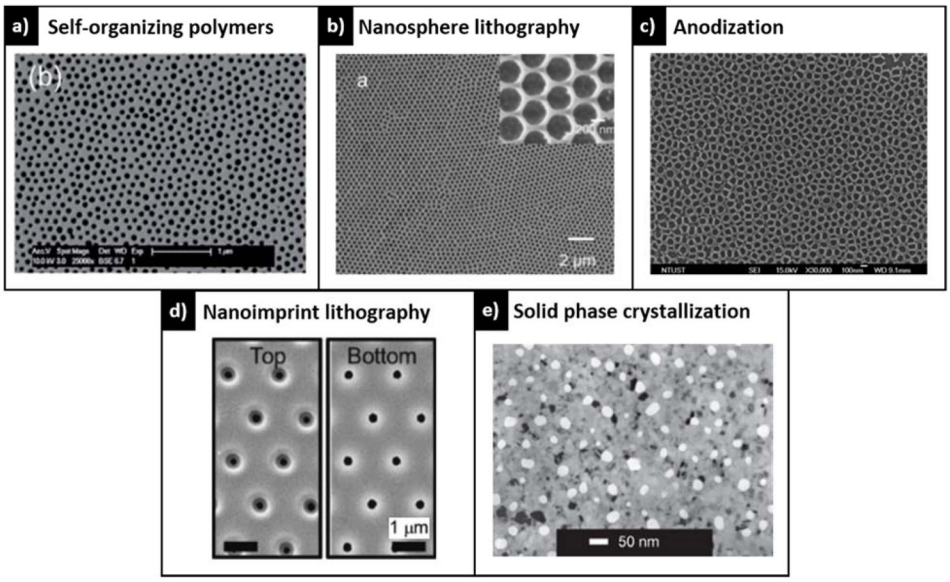

Figure 2.

Micrographs corresponding to fabricated membranes: a) SiN membrane by self-organizing polymers adapted from Ref. [5]; b) polyethersulfone membrane by nanosphere lithography, adapted from Ref. [44]; c) aluminum oxide membrane by anodization, adapted from Ref. [45]; d) polystyrene membrane by nanoimprint lithography, adapted from Ref. [22]; and e) silicon membrane by solid phase crystallization, adapted from Ref. [4].

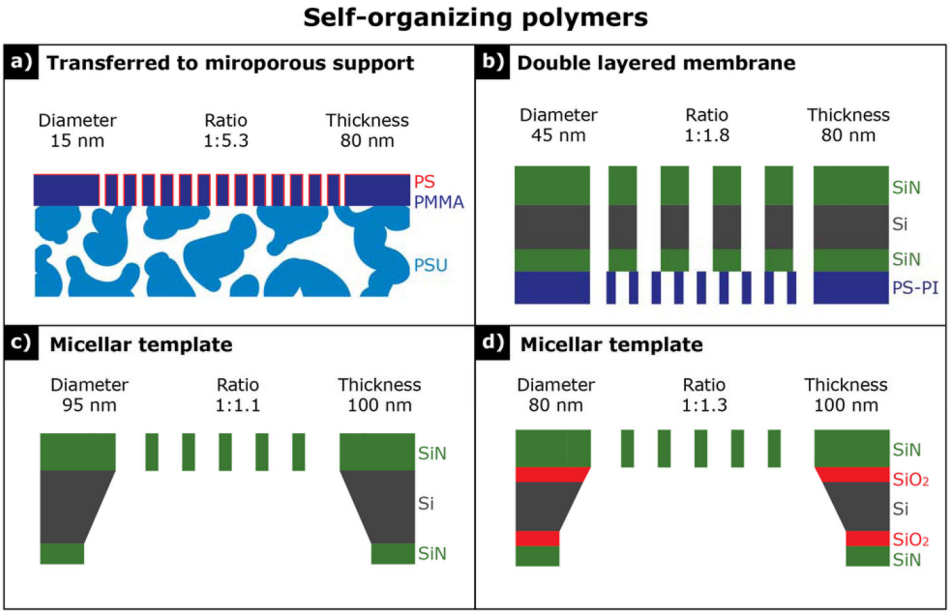

Figure 3.

Cross-sectional schemes of nanoporous membranes fabricated through self-organizing polymers: a) PS-PMMA membrane transferred onto a microporous polymeric substrate [50]. b) PS-PI membrane supported on a microporous silicon membrane [51], c) SiN membrane fabricated from a micellar monolayer assembled on a 47Prime; Si wafer [5], and d) SiN membrane fabricated over a 47Prime; Si wafer yielding 145 chips 10x10 μm^2 [52].

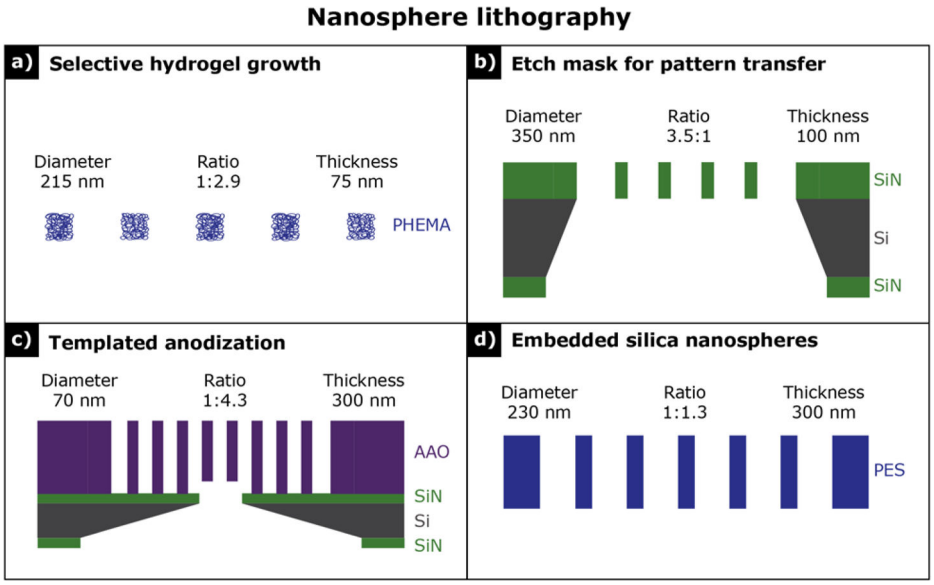

Figure 4.

Cross-sectional schemes of nanoporous membranes fabricated through NSL: a) PHEMA hydrogel brush membrane fabricated using PS nanospheres [60], b) SiN membrane fabricated through a Cr etch mask produced from PS nanospheres [61], c) aluminum oxide membrane fabricated by patterned anodization through PS nanospheres [62], and d) polymeric membrane lifted-off from its processing substrate by dissolving a cellulose acetate sacrificial layer [44].

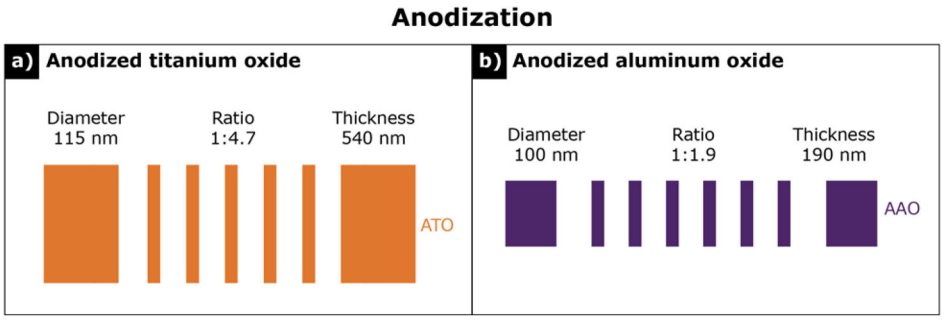

Figure 5.

Cross-sectional schemes of nanoporous membranes fabricated through anodization: a) ATO membrane transferred through lift-off [69] and b) AAO membrane used as template for the fabrication of silver nanoparticles [45].

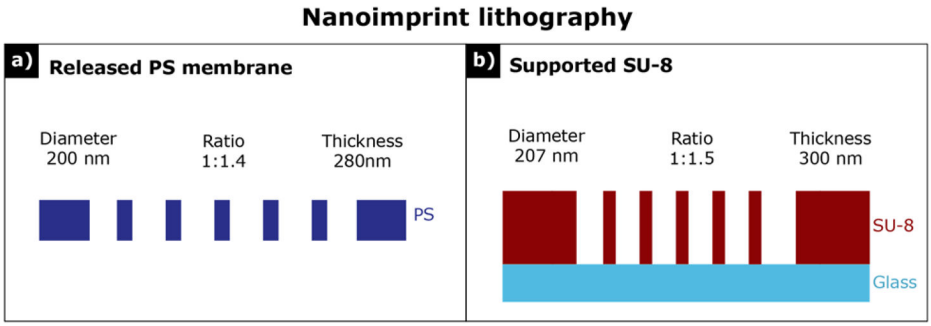

Figure 6.

Cross-sectional schemes of nanoporous membranes fabricated through nanoimprint lithography: a) PS nanoporous membrane fabricated by capillary force nanoimprint lithography and released through dissolution of PSS film [22] and b) SU-8 porous film imprinted through an AAO template [88].

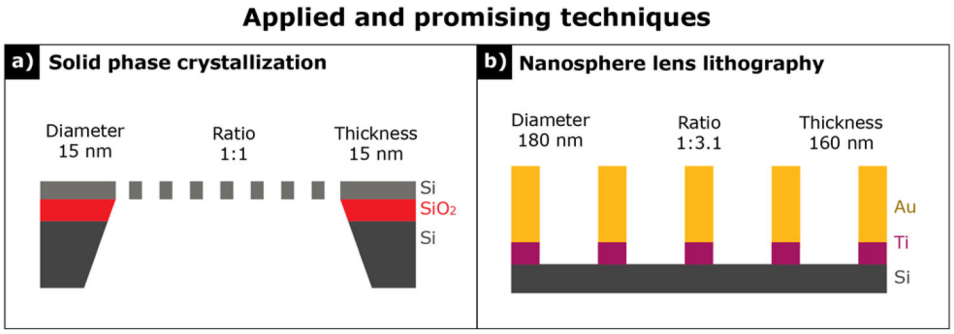

Figure 7.

Promising techniques for nanoscale patterning: a) free-standing Si membrane successfully fabricated through the solid phase crystallization of a Si thin film [4] and b) nanoporous pattern developed on Au/Ti stack through nanosphere lens lithography [104].

Table 1

Comparison of techniques resulting in free-standing or released membranes with a pore size to thickness aspect ratio close to one

Technique	Pore dimension (nm)		Aspect ratio (size: thickness)
	Size	Thickness	
Self-organizing polymers	15 – 95	80 – 100	1 – 1:5
Nanosphere lithography	70 – 350	75 – 500	1:1 – 3.5:1
Anodization	100 – 115	190 – 540	1:2– 1:3
Nanoimprint lithography	200	280	1:1.4